Aging aerosol in a well-mixed continuous flow tank reactor: An introduction of the activation time distribution

Franz Friebel, Amewu A. Mensah

Institute for Atmospheric and Climate Science, ETH Zurich, Zurich, 8092, Switzerland

5 *Correspondence to*: Franz Friebel (franz.friebel@env.ethz.ch) and Amewu A. Mensah (amewu.mensah@env.ethz.ch)

Abstract. Simulating atmospheric aging processes in the laboratory under atmospheric conditions typically requires large aerosol chambers (several m^3) in order to achieve extended observation times. We developed an experimental approach that enables long observation times in small chamber volumes by operating the aerosol chamber in a Continuous Flow Stirred Tank Reactor (CSTR) mode. We present a mathematical framework which allows the retrieval of data beyond calculating mean

10 values using the newly introduced metric activation time (t_{act}). This concept was developed and successfully tested to characterize the change in cloud condensation nuclei (CCN) activity of soot particles due to heterogeneous oxidation with ozone. We show that this concept can be applied to other systems investigating non-gradual transitions. The change in CCN-activity was parameterized with t_{act} and agreed well with theoretical predictions. Furthermore we show how t_{act} can be applied for the analysis of data originating from other oxidation flow reactors widely used in atmospheric sciences. This concept allows

15 to explain discrepancies found in intercomparison of different chambers.

1 Motivation

Aerosol particles undergo various chemical reactions and physical modification processes once they are emitted into the atmosphere. The time scale for such reactions and processes depends on the atmospheric lifetime of the individual aerosol species. For example sea salt particles have a lifetime of approximately 0.4 days, soot particles can have a lifetime of more

20 than a week (Textor et al., 2006). Simulating atmospheric aging as realistically as possible is essential to understand the true impact of different pathways of ambient particle processing. This includes the fate of aerosol particles in the atmosphere and their potential to form clouds, an important parameter for climate and weather. Mimicking extended aging times is one of the most challenging task for the investigation of aerosols under laboratory conditions (Burkholder et al., 2017). There are two common approaches to solve this problem. One is to store the aerosol of interest in large chambers to achieve long observation

25 times. Here aging durations of 16 hours at atmospherically reactant concentrations can be achieved, which has been shown e.g. for the SAPHIR chamber of FZ Julich with a volume of 270 m^3 (Rohrer et al., 2005; Rollins et al., 2009) but extending the observation time by increasing the tank volume is often technically and economically not feasible. The second option is to increase the concentration of the reactive compounds such as oxidants and aerosol particles, in order to reduce the reaction time (Kang et al., 2007; Keller and Burtscher, 2012). However, in these cases the reactant concentrations can be elevated by

several orders of magnitude in comparison to the atmosphere. Thus, the results of such experiments can be misleading with respect to their atmospheric relevance because the aerosols aging rates are not always directly proportional to the concentration of the oxidants. Further, the aging pathways can differ significantly in addition to the perturbed partitioning of reactive species and products (McNeill et al., 2007; Donahue et al., 2006).

5 Below we present an experimental approach that can be used to achieve long aerosol aging times with neither need for large chamber volumes nor high reactant concentrations. The continuous flow stirred tank reactor (CSTR) describes an aerosol chamber, which is continuously filled with an aerosol flow constant in composition over time. The aerosol inside the CSTR is perfectly mixed, therefore a mix of aged and unaged aerosols is continuously extracted from the CSTR for analysis. This approach is close to real processes in the atmosphere where aerosols are constantly emitted, mixed and removed as well. The

10 CSTR is able to maintain stable and constant operation condition over unlimited time scales in steady state. The steady state in the CSTR is characterized by constant concentration of all compounds and constant reaction rates. It should be noted that the age of an aerosol is thereby not directly proportional to the experimental duration.

This concept has been applied in the field of chemical engineering for a long time (Cholette and Cloutier, 1959). One of the

15 reasons for its limited application in atmospheric science might be the increased complexity in data analysis in comparison to batch-experiments. In this reactor concept an aerosol flow is continuously fed-in as well as withdrawn with equal flow rates while the reaction takes place. While changes in aerosol concentration or particles growth due to sample withdrawal, wall-losses and coagulation can be well described by theoretical concepts (Levenspiel, 1999; M. Kuwata, 2012; Crump and Seinfeld, 1980) limited theoretical descriptions seem to exist for non-gradual transitions of the aerosol particle such as CCN activation.

20 In the following, we discuss a theoretical foundation for the experimental analysis of non-gradual transitions in a CSTR. For this we developed mathematical frameworks which allows the retrieval of characteristic parameters from the system of interest and which allows for the prediction of the response function of the CSTR. This includes an idealized system where the parameter of interest can be described with one number as well as a more realistic situation where there is a distribution of the parameter of interest. Additionally we apply this concept to other types of continuous flow aging chambers and show how

25 varying residence time distributions lead to different results at similar experimental conditions.

2   Introduction of the CSTR

Often laboratory studies have been complemented by field measurements and modelling studies to better understand
30 atmospheric aging of aerosols. Designing experiments in the laboratory involves mimicking atmospheric processes as closely as possible under as realistic conditions as achievable in a laboratory setting. The benefit of this approach is that the investigation of reactions is not dependent on several uncontrolled parameters such as meteorological conditions e.g. wind

direction, wind speed, or air parcel mixing. Further, process variables, for example, reactant concentrations can be actively and therefore systematically modified to allow for a detailed investigation of their effects. Such type of experiments are typically performed by creating an artificial atmosphere within reactors. From the physico-chemical perspective, generally three types of reactors are distinguished: the batch-reactor, the plug flow or flow tube reactor and the Continuous Flow Stirred

5 Tank Reactor (CSTR).

In a batch-reactor the reactants are introduced at the beginning of the experiment aiming for homogeneity and then the reaction is allowed to procede. The composition throughout the vessel is homogeneous but evolving in time, therefore no steady state conditions are ever achieved. After a certain reaction time the sample is discharged or collected and subjected to further analysis. A flow tube is a steady state reactor in which no mixing along the flow path takes place resulting in a constant output

10 of products depending on the residence time within the reactor. The CSTR is a steady state reactor as well but opposite to the flow tube the volume is stirred to achieve a homogeneous composition throughout the reactor volume. In addition, a continuous feed-in of reactants and withdrawal of sample rate take place at the equal flow rates simultaneously. Due to the mixing, sample stream conditions are the same as within the reactor and the sample itself is characterized by a constant composition.

The concept of the CSTR requires perfect internal mixing. Due to the good miscibility and low viscosity of gases and the

15 aerosol particles being homogenously dispersed it is a valid assumption for the concepts presented herein. Especially in the case of mimicking atmospheric processes, the time needed for dissipating all gradients can be considered small in comparison to residence times of several hours. Starting with a reactant free gas phase within the CSTR, the aerosol is fed into the chamber, referred to as filling regime. Once the equilibrium is reached, the CSTR is kept in a dynamic equilibrium, to which we refer to as steady state regime. During a subsequent flushing regime, the aerosol is flushed out with reactant free gas. Each of these

20 regime can be used independently for data analysis and is indicated at the top of Fig.3.

The key parameter for the description of reactions within a CSTR is the hydrodynamic mean residence time (τ_{CSTR}). It can be obtained from the reactor volume (V_{CSTR}) and the volumetric flow through the CSTR ($\dot{V}$) as shown in eq. (1) (Levenspiel, 1999)

$$\tau_{\mathrm{CSTR}} = \frac{V_{CSTR}}{\dot{V}} \tag{1}$$

25 ## 2.1 Filling regime

During the filling regime the aerosol particle concentration in the CSTR increases continuously until it reaches a stable concentration. The change in aerosol particle concentration ($[\mathrm{A_{CSTR}}(t)]$) can be calculated as function of the experimental duration (t) by eq. (2), where ($[\mathrm{A_{feed\text{-}in}}]$) describes the aerosol concentration in the feed-in flow.

$$[\mathrm{A_{CSTR}}(t)] = [\mathrm{A_{feed\text{-}in}}] \cdot \left(1 - e^{\left(\frac{-t}{\tau_{\mathrm{CSTR}}}\right)}\right) \tag{2}$$

We assume that the CSTR reached steady state when the difference between $[A_{CSTR}(t)]$ and $[A_{feed-in}]$ is smaller than the resolution of the analytical instruments used. Here we chose the fourfold mean residence time (4τ criterion) as reference point for the start of the steady state. At this point the difference between $[A_{CSTR}(t)]$ and $[A_{feed-in}]$ is less than 2% which is lower that the resolution of most aerosol particle counters.

5   2.2   Steady state

The steady state is the part of the filling regime where the CSTR is a dynamic equilibrium. All processes and reactions continue but the concentrations of all compounds remain constant over time. In theory, the operation point can be maintained for an infinite timespan. It is important to note that the experimental duration is not the same as the aging time of the aerosol, which is in contrast to experiments in batch-chambers.

10   As a result of the continuous feed-in and flush-out flow, different aerosol fractions that enter the CSTR at different times are present simultaneously, resulting in a residence time distribution (RTD). In CSTRs the RTD can be described by eq. (3) and is plotted in Fig. 1 (dashed line / steady state). With an increasing individual residence time (also denoted as particle age) the share of aerosol fractions declines exponentially. The individual residence time of a specific particle fraction is indicated by the color coding Fig. 1. The individual share of particles of a specific residence time can be calculated by integrating RTD

15   over time (eq. (4)) leading to the residence time sum distribution RTD_{sum} represented by the area under the curve.

$$RTD(t)= e^{\frac{-t}{\tau_{CSTR}}} \tag{3}$$

$$RTD_{sum}(t)= \int_0^\infty RTD(t)\ =1-e^{\frac{-t}{\tau_{CSTR}}} \tag{4}$$

2.3   Flushing regime

From the point that no fresh aerosol but only particle free air is added, the CSTR operates in the flushing regime. This operational mode is similar to batch-aerosol chambers where the aerosol is flushed out continuously.

The initial RTD at the switching point (t_{switch}) and therefore the ratio between younger and older aerosol fractions is preserved,

20   but the individual residence time rises simultaneously for all particles with flushing duration. In other words: All particles age simultaneously. Figure 1 illustrates how the RTD changes in the flushing regime. Each color in the area represents an individual aerosol fraction with a defined residence time. Blue stands for the lowest and red for the highest residence times. The curve labeled with "steady-state" represents the RTD in steady-state while the other curves show the RTDs for additional time increments after the flushing regime has been initiated.
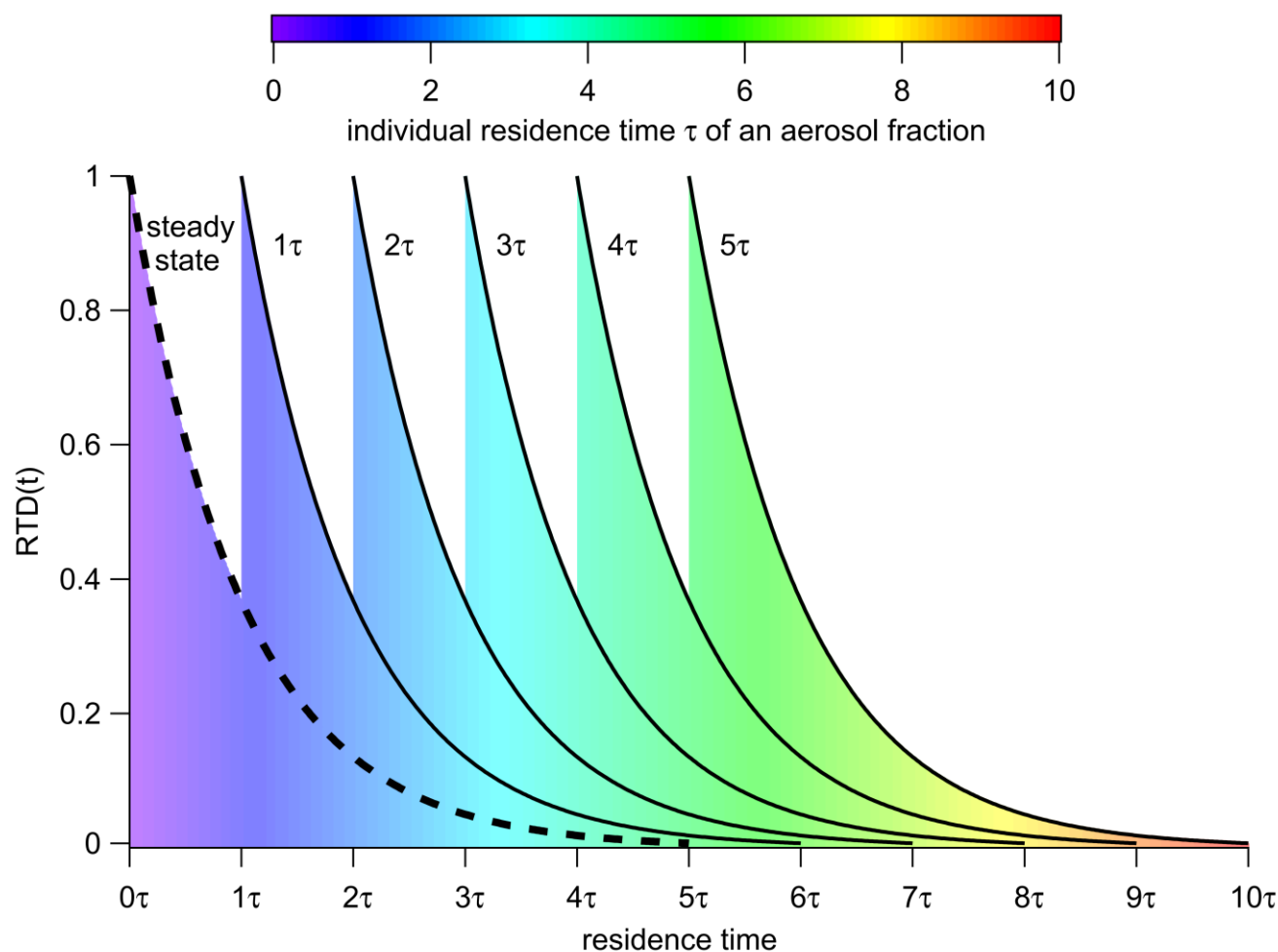
Figure 1: RTD inside the CSTR for steady state and for different time steps (multiples of τ) while flushing the CSTR. The area below the curve is proportional to the fraction of aerosol particles at a specific residence time. The individual residence time of a specific particle fraction is indicated by the color coding.

5   At the same time the aerosol concentration ($[A_{CSTR}(t)]$) is declining exponentially in the flushing regime and can be calculated using eq. (5). The initial aerosol concentration in the CSTR is the aerosol concentration at the switching point ($[A(t=t_{switch})]$). In case the flow rate of the flush flow is altered compared to the previous regimes, τ_{CSTR} would change as well but the RTD would not be affected.

$$[A_{CSTR}(t)]=[A(t=t_{switch})] \cdot e^{\left(\frac{-t}{\tau_{CSTR}}\right)} \tag{5}$$

2.4 Comparison with aerosol aging experiments in batch-mode

The use of a CSTR provides additional opportunities in performing aerosol aging experiments, but comes with a more complex experimental setup compared to aerosol tanks that are run in batch-mode.

An ideal batch-aerosol tank has to be filled instantly, but in practical this ideal filling procedure is almost impossible to be
5 achieved. If the filling time is short compared to the total aging time, the initial RTD can be ignored in data analysis. In contrast to that, the filling of the chamber is already part of CSTR experiments and data analysis can be performed on the partially aged aerosol. The flushing regime in both tank types is similar, but at the start of the flushing, the aerosol inside the CSTR is already partly aged in a defined way. Therefore, the maximum average aging time in CSTR experiments is higher than in batch-mode experiments.

3 Introduction of the activation time (t_{act}) for non-gradual transitions

The concept of the CSTR requires a different approach to interpret the measured data than data from batch-mode experiments, due to the non-uniform residence time distribution. While there are concepts to describe continues changes on the level of single particles in CSTRs (e.g. condensational growth (Kuwata and Martin, 2012)), so far there is no concept that describes
15 non-gradual transitions (in atmospheric sciences) to the best of the knowledge of the authors .

Non-gradual transitions describe a step-wise change in a particle property as function of an external parameter. For example, some aerosol particles exhibit a significant change in diameter due to deliquescence and efflorescence as a function of relative humidity. Similarly, the change from cloud condensation nuclei (CCN) to activated droplets due to exposure to a super-critical super saturation can be considered a non-gradual change.

20 If the all other parameters stay constant, while a particles undergoes changes that result in a non-gradual transitions, this transition can be described as a function of time. We define the required time span or necessary aging time that leads to a change in a specific particle property, causing the non-gradual transition as activation time (t_{act}).

For the further discussion we focus on the example of an aerosol particle aging process resulting in an increased CCN-activity. The aging process is a continuous and irreversible process that changes how a single particle can accumulate water at super
25 saturated conditions. Once a particle reaches the necessary aging time t_{act} it is considered to be CCN-active at a respective super saturation.

In the real world, no non-gradual transitions can be found, however some changes occur on a short time scale with respect to the time resolution of the measurement or detection, respectively. Thus it is a valid simplification to consider such changes as instantaneous.

30

3.1 Aerosol particle activation and activation time in a CSTR

The fraction of particles acting as CCN (activated fraction; *AF*) is defined as the ratio of activated particles divided by the total number of particles in the sample volume. The measured *AF* can be used to obtain the activation time t_{act} and to predict the theoretical *AF* throughout the entire experiment. Hereby the three different regimes (filling, steady state, flushing), have to be

5   treated individually.

3.1.1 Particle activation during filling regime

Assuming that only aerosol particles are CCN-active with an individual residence time in the aerosol chamber higher than t_{act}, eq. (6) can be derived for two different experimental durations. If the experimental duration *t* is below t_{act} the *AF* is 0, if *t* is above t_{act} the *AF* is greater than 0. Converting eq. (6) into eq. (7) allows the calculation of the activation time t_{act} throughout

10   the filling and steady state regime.

$$t \leq t_{act}: \quad AF(t) = 0$$
$$t > t_{act}: \quad AF(t) = \frac{\text{activated particles}}{\text{all particles}} = \frac{RTD_{sum}(t) - RTD_{sum}(t=t_{act})}{RTD_{sum}(t)} \quad (6)$$

$$t_{act} = \ln\left(1 - \left((1 - AF(t)) \cdot \left(1 - e^{\frac{-t}{\tau_{CSTR}}}\right)\right)\right) \cdot -\tau_{CSTR} \quad (7)$$

3.1.2 Particle activation during steady state regime

After the conditions in the aerosol chamber reached steady state, the measured *AF* does not change anymore. Again, this is due to the continuous addition of fresh particles and withdrawal of sample volume resulting in a constant RTD. Therefore, eq.

15   (7) can be simplified to eq. (8) taking the following limit into account: $\left(\lim\limits_{t \to \infty} eq.\ (7) = eq.\ (8)\right)$

$$t_{act} = -\ln(AF) \cdot \tau_{CSTR} \quad (8)$$

It is important to keep in mind, that there is no linear correlation between *AF* and t_{act}. The change in *AF* is not proportional to the change in t_{act} induced by different experimental conditions or by measuring the *AF* at a different super saturation (SS). Figure 2 shows the RTD inside a CSTR that is in steady state (black curve). The area under the curve represents the total

20   particle population inside the CSTR. The blue striped area represents the fraction of particles that are CCN-active for 3 different pairs of t_{act} and *AF*.
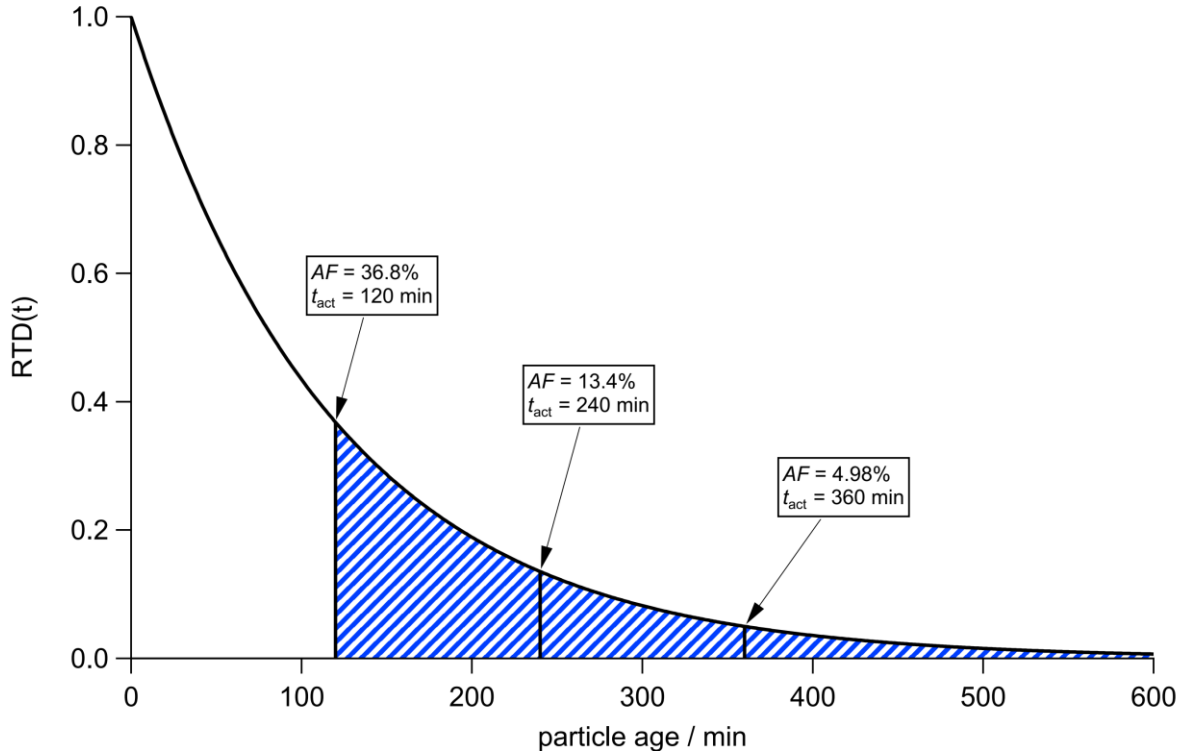
Figure 2: Correlation between *AF* and *t*ₐcₜ for a CSTR in steady state with τ_{CSTR} = 120 min.

3.1.3 Particle activation during flushing regime

5   In the flushing regime, no fresh particles are added and all aerosol particles age simultaneously. As shown in Fig. 1 the RTD of the particle population is shifted towards longer aging times. Thereby the fraction of particles that cross a certain t_{act} increases. This leads to an exponential increase of the *AF* inside the CSTR (global *AF*) until *AF*=1. From a graphical perspective, the increasing *AF* can be described by centering the RTD function (eq. (3)) at t_{switch}, the time at which the aerosol chamber is switched to the flushing-regime. Based on this assumption and eq. (6) we can develop eq. (9).

$$\mathrm{AF}(t)_{\mathrm{flushing}} = \int_{t_{switch}/\tau}^{t/\tau} e^{\left(\frac{t-2*t_{switch}}{\tau}\right)} \, d\left(\frac{t}{\tau}\right) \tag{9}$$

10   However, eq. (9) only describes the fraction of particles that are older than t_{switch} and therefore the global *AF* only if $t_{act} = t_{switch}$. To determine the *AF* for conditions when $t_{act} < t_{switch}$ ($AF(t=t_{switch}) > 0$) or for a delayed activation, $t_{act} > t_{switch}$, a new parameter t_{offset}, is introduced. This parameter is an offset of the *AF*-curve along the time-axis. Taking t_{offset} into account, eq. (10) can be obtained after integrating eq. (9).

$$AF(t)_{\text{flushing}} = e^{\left(\frac{t\, +\, t_{\text{offset}}\, -\, 2\cdot t_{\text{switch}}}{\tau_{\text{CSTR}}}\right)} - e^{\frac{t_{\text{switch}}}{\tau_{\text{CSTR}}}} \tag{10}$$

The parameter t_{offset} is initially unknown and has to be calculated. For this the AF at $t = t_{\text{switch}}$ is taken and eq. (10) is solved for t_{offset} (eq. (11)).

$$t_{\text{offset}} = \ln\left(AF(t{=}t_{\text{switch}}) + e^{\frac{t_{\text{switch}}}{\tau_{\text{CSTR}}}}\right)\cdot \tau_{\text{CSTR}} + t_{\text{switch}} \tag{11}$$
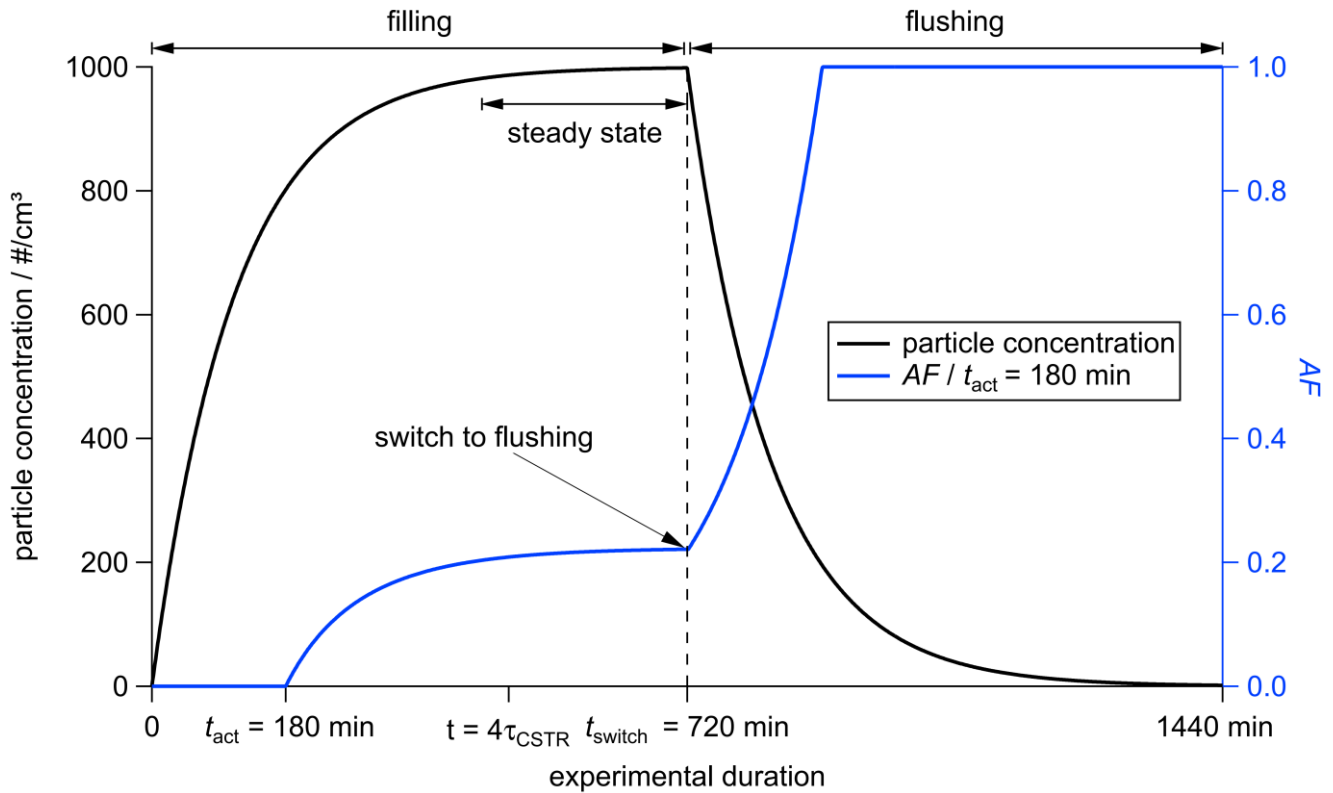
Figure 3: Theoretical change of the activated fraction and particle concentration throughout filling, steady state, and flushing regime.

With these equations the AF and the particle number concentration inside the CSTR can be calculated throughout all

10 experimental stages. Figure 3 shows how the AF (blue, right axis) and the particle number concentration (black, left axis) change during an experiment with $\tau_{\text{CSTR}} = 120$ min, $t_{\text{act}} = 180$ min and $[A_{\text{feed-in}}] = 1000$ cm^{-3}. A detailed description of all stages is listed in Table 1.

Table 1: Comparison of the aerosol concentration and the *AF* in different CSTR-regimes

	time scale	*AF inside CSTR*	*aerosol particle concentration*
filling	start - 480 min / 4τ	*AF* is 0 % at the start. After crossing t_{act} increasing AF with constantly declining growth rate.	Increasing particle concentration with constantly declining growth rate.
steady state	480 to 720 min	*AF* reaches a stable value of 22.1 %.	Aerosol concentration is constant, changes are below the detection limit.
flushing	720 min - end	Exponential increase of *AF* until reaching 100 %.	Exponential decline of the aerosol concentration.

4 Application in first experiments

4.1 Introducing the activation time distribution $P(t_{act})$

The approach discussed so far is based on the assumption that all aerosol particles are identical and therefore a specific property of the whole aerosol population can be described with a single parameter. However, this is rarely as in reality an aerosol population consists of aerosol particles, whose properties are typically distributed around a mean-value (e.g. the mode of a particle size distribution). While the aerosol population might be mono-modal and narrowly-distributed with respect to one parameter such as the aerosol particle's electrical mobility diameter, it can be multi-modal and broader distributed with respect to another parameter (e.g. aerodynamic diameter). Therefore, it has to be expected that the activation time (t_{act}) shows the same behavior. For this we introduce the activation time distribution $P(t_{act})$ and discuss its theoretical impact on non-gradual transitions in CSTR-experiments.

4.2 Impact of the activation time distribution on the global *AF*

In the previous section it was shown how the global *AF* evolves throughout a whole CSTR-experiment (blue curve in Fig. 3). This curve was calculated based on the assumption of ideality, i.e. every aerosol particle that is older than $t_{act} = 180$ min activates. While, this assumption can be valid for some cases it surely cannot be representative for all real-world conditions. To discuss the impact of an activation time distribution $P(t_{act})$ on the evolution of the global *AF* in a CSTR we consider a model system with $P(t_{act})$ representing a Gaussian distribution with a mean (μ) of 180 min and a standard deviation (σ) of 30 min (eq. (12)).

$$P(t_{act}) = \frac{1}{\sqrt{2\pi\sigma^2}} e^{-\left(\frac{(t_{act}-\mu)^2}{2\sigma^2}\right)} \tag{12}$$

In a CSTR particles with different individual residence times are present at the same time. For a better understanding the "individual residence time of a particle" will be referred to "particle age" from here on. With an increasing particle age the fraction of particles declines in a CSTR during steady state (Graph A, Fig. 4). Parallel to that, the activation time distribution $P(t_{act})$ is the same for all particles (Graph B, C, D in Fig. 4), regardless of their age. The fraction of activated particle inside

5 the CSTR (global AF) therefore has to be described as an overlap of the RTD and $P(t_{act})$. On the one hand, old particles with a long individual residence time can be fully activated, but contribute only little to the total particle population (Graph D in Fig. 4). On the other hand, young particles with a short individual residence time contribute largely to the total particle population but only a small fraction is activated (Graph B in Fig. 4). If the particle age is equal to the mean value of a Gaussian $P(t_{act})$, then half of the particles will be activated (Graph C in Fig. 4). The area under the curves in graph B, C, and D are proportional

10 to their relative abundance during steady state. The red area shows the fraction of activated particles within this specific population.
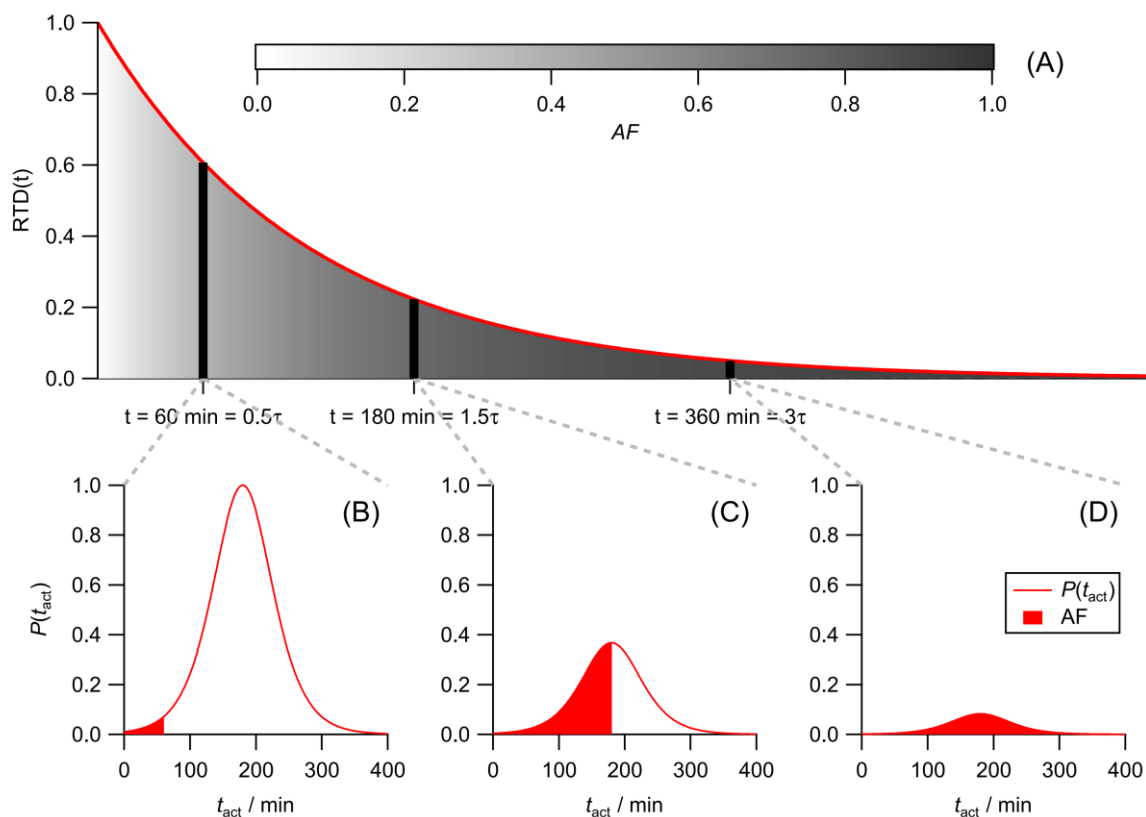
Figure 4: (A): The RTD in steady state is shown (red line). The grey shaded area underneath the curve represents the increasing fraction of activated particles with increasing particle age.

(B-D): Activation time distribution at different particle ages. The total area under the activation time distribution curve represents the relative abundance of particles at their specific age. The red-colored area represents the fraction of activated particles within the population of this particular particle age.

4.3   Calculation the total activated fraction

5   The global AF for each point in time can be obtained by calculating the change in $AF(t_{act},t)$ for each individual t_{act}, multiplied with the relative abundance of particle with this t_{act} $P(t_{act})$ and integrated over the whole range of possible t_{act}'s. (lower limit: $t_{act} = 0$ min; upper limit: $t_{act} = t$)

$$AF(t) = \int_{t_{act}=0}^{t_{act}=t} AF(t_{act},t) \cdot P(t_{act}) \ dt_{act} \tag{13}$$

In Fig 5 the difference in the evolution of the global AF within a CSTR ($\tau_{CSTR} = 120$ min) in the case of two different $P(t_{act})$ is

10   presented. The blue curve is the same as in Fig. 3 postulating all particles activate uniformly at $t_{act} = 180$ min ($AF_{step}(t)$, $P_{step}(t_{act})$). The red curve shows the global AF for a Gaussian shaped activation time distribution like in Fig. 4 with $\mu = 180$ min and $\sigma = 30$ min ($AF_{gaussian}(t)$, $P_{gaussian}(t_{act})$). While the uniform scenario shows no activity be for reaching t_{act}, the Gaussian distribution scenario shows an earlier activation onset (t_{act} – onset). This is because there are some particles in the population, that activate earlier than the mean activation time. e.g. all particles within the red area left of $\mu = 180$ in Fig. 4 B - D. Both

15   curves reach a constant global AF during steady state, but in the Gaussian distribution scenario the AF is higher ($AF_{gaussian} = 0.242$ vs $AF_{step} = 0.221$). In the flushing regime the AF grows exponentially in both scenarios, but in the Gaussian distribution scenario full activation is reached later than in the uniform scenario. Generally, a broader $P_{gaussian}(t_{act})$ leads to an earlier t_{act} – onset while full activation is reached later because the broader distribution extends over a wider range of individual t_{act}'s on the single particle level.
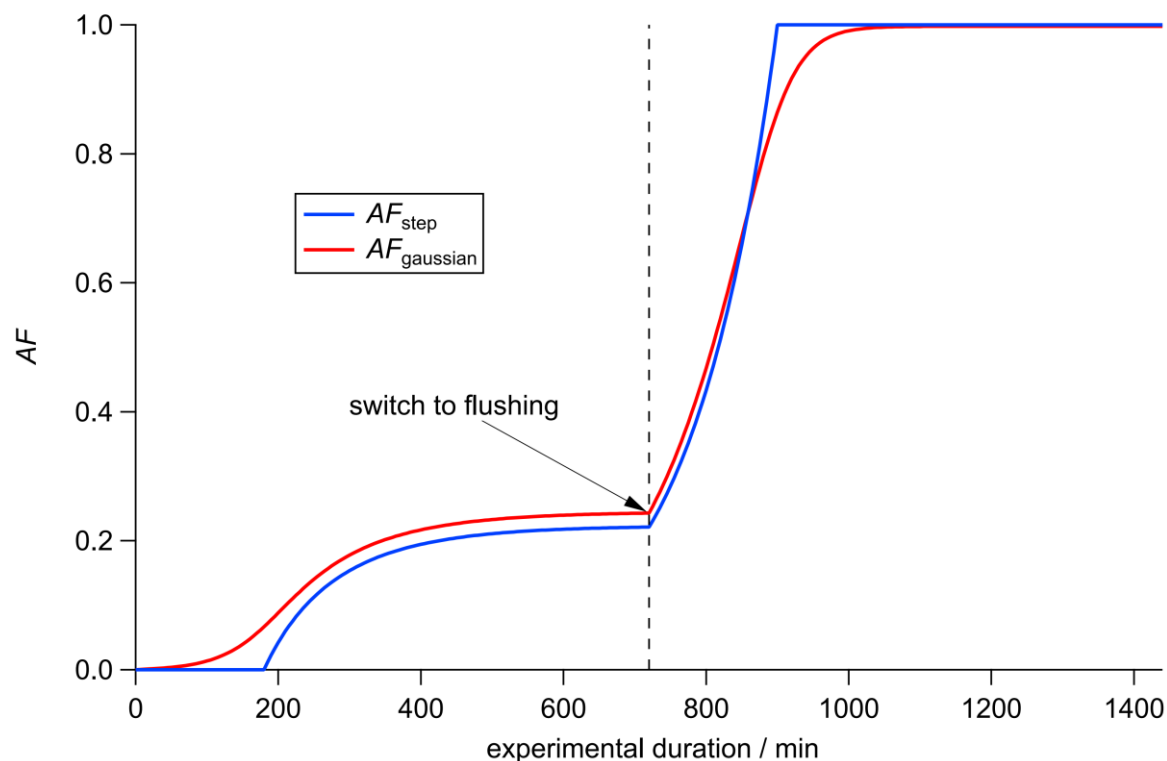
Figure 5: *AF* response function inside a CSTR for a uniform aerosol population (blue) and an aerosol population with an activation time distribution represented by a Gaussian distribution (red).

4.4   Equivalent parameters t_{act} – onset and t_{act} vs $t_{act}0.5$

5   In the literature, different parameters are used to describe the activation of particles. In the case of CCN-activation it is either an SS-onset often characterized by a minimum threshold (e.g. 1 % *AF*) or a critical SS, when 50 % of the particles activate. Here t_{act} is a third parameter, but the equivalent parameters t_{act}-onset and $t_{act}0.5$ can be obtained as well. Following the aforementioned nomenclature in the CCN community, we define t_{act}-onset as the time when the global *AF* inside the CSTR crosses a defined value, here *AF* = 1%. Similarly, we define $t_{act}0.5$ as the time after which 50 % of the initial particle population

10   is activated. In Table 2 the three parameters for t_{act} are compared for the two scenarios.

Table 2: Influence of the t_{act}-distribution on the t_{act}-onset, tact and critical-t_{act}.

		$P_{step}(t_{act})$	$P_{gaussian}(t_{act})$
t_{act}-onset	$AF = 1$ % inside the CSTR (global *AF*)	185 min	87 min
t_{act}	Obtained from the *AF* in steady state in Fig. 5 using eq. (8) $AF_{step} = 0.221$; $AF_{gaussian} = 0.242$	180 min	170 min
$t_{act}0.5$	Obtained from $P(t_{act})$	180 min	180 min

At first glance, the values of the different t_{act}s differ significantly potentially indicating that the CSTR-approach and the activation time concept presented here have severe short comings compared to already established approaches e.g. oxidation flow reactors (OFR). However, the presented deviations are solely caused by the considered distributions of the activation time and affect OFRs as well. First it should be mentioned, that t_{act}-onset, t_{act}, and $t_{act}0.5$ are determined from different parameters

5   each. While t_{act}-onset is determined with respect to the entire population within the CSTR, t_{act} is based on a theoretical calculation taking the global AF in steady state into account, and in the case of $t_{act}0.5$ only the particle activation distribution $P(t_{act})$ is considered ignoring the contribution of the specific share of particles to the entire population within the CSTR. As there is a significant share of particles activating significantly earlier than the nominal activation time ($\mu = 180$) in the case of a Gaussian distribution a fraction of 1 % of the entire particle population within the CSTR is already activated after 87 min.

10   Opposite to this, the threshold value of 1 % is crossed later than the nominal activation time in the case of the step distribution because even though every single particle activates after exactly 180 min of aging, it takes some additional time before a fraction of 1 % of the entire particle population within the CSTR is older than 180 min. The difference in tact of 10 min between the two P(tact)-approaches is due to the application of eq. (8). This equation is in strict sense defined for the ideal step function only. Therefore calculation of tact from the higher AF in steady state for Pgaussian(tact) has to lead to a lower

15   tact value compared to Pstep(tact).As can be seen in Graph C of Fig. 4 50 % of the particles with a residence time equal to the nominal activation time are activated in the case of a Gaussian distribution corresponding to $t_{act}0.5$. In the case of a step function, all particles are activated once the respective particle population is older than tact. In the following it will be shown that $P(t_{act})$ can be retrieved from CSTR-experiments.

5   Application to experimental data

20   In the laboratories at ETH Zurich we performed aging experiments in a 2.78 m³ stainless steel aerosol chamber run in CSTR mode. We investigated the change in CCN-activity of soot particles rich in organic carbon from propane combustion (miniCAST, set point 6) due to heterogeneous ozone oxidation. The particles were size selected at 100 nm by a Differential Mobility Analyzer (DMA). These size selected aerosol particles were diluted with particle free and VOC-filtered air in order to achieve a constant aerosol flow of 25 lpm with a particle concentration in the range of 1000 to 1500 cm⁻³ depending on

25   experiment day. The aerosol flow was fed into the aerosol chamber, where a constant Ozone concentration of 200 ppb was maintained throughout the entire experiment. Downstream of the aerosol chamber the CCN-activity was measured with a cloud condensation nuclei counter (CCNC; Roberts and Nenes, 2005). The size distribution data was acquired by a scanning mobility particle sizer (SMPS) system from which the the total particle concentration could be derived. The data was analyzed focusing on the three following aspects:

30   1) Can the aerosol chamber be operated in CSTR-mode for up to 12 h which requires a constant aerosol feed-in flow and a perfect internal mixing?
         2) Can the change in CCN-activity of soot particles due to oxidation with ozone be investigated with CSTR-mode aging experiments?

3)   Can t_{act} and its distribution ($P(t_{act})$) be retrieved from experimental data?

In Fig. 6 two data sets for two experiments conducted on two different days are shown. Both experimental setups differ only by the super saturation conditions set in the CCNC (A: 1.0 %, B: 1.4 %). The graphs A1 and B1 show the particle concentration (black crosses; left axis), the measured AF (red crosses) and the fitted AF (blue dashed line, both right axis). The graphs A2

5   and B2 show the $P(t_{act})$ (blue solid line) retrieved from fitting the measured AF. The particle concentration curves follow the theoretical filling and flushing curves in a CSTR. The slight decline in the concentration observed in the region where steady state is expected in graph A1 is due to a slight but undesired reduction in the feed-in flow that was experienced during the experiment. The measured particle flush rate τ_{flush} obtained during the flushing regime is 104 min in both experiments, which differs slightly from the theoretical flush rate $\tau_{CSTR} = 111$ min. This difference is caused by particle losses to the chamber wall.

10   From this difference the particle wall loss rate of $k = 0.000625$ min^{-1} and a mean particle life time upon wall loss of 1600 min was determined assuming first order loss rates. Based on the theoretical discussion above, the measured AFs (red crosses) show the expected change throughout the entire experiment. In the beginning of both experiments the AF is 0. After a minimum aging time each AF starts to increase until it reaches a constant level (A1: $AF = 0.091$, 1.0% SS; B1: $AF = 0.233$, 1.4% SS). In the flushing regime, each measured AF increases exponentially until it reaches a value of 1. The gaps in the curves during

15   steady state are due performing measurements at other SS.

The $P(t_{act})$ presented in A2 and B2 of Fig. 6, respectively, were obtained by performing a curve fitting operation assuming $P(t_{act})$ to be a mono-modal Gaussian distribution and with the parameters μ ($= t_{act}0.5$) and σ to be optimized. As can be seen in Table 3 as well as in A2 and B2 of Fig. 6, μ as well as σ are larger for $P(t_{act})$ at a 1.0 % SS of compared to the results obtained for 1.4 % SS. The mean activation time being larger for 1.0 % indicates that the longer the chemical aging proceed the initially

20   inactive soot particles activate a at lower SS. In addition, we list t_{act} obtained from the AF during steady state in Table 3. The instrumental uncertainty for obtaining t_{act} from steady state using eq. (8) is $\pm$ 11.6 min. The differences between t_{act} and $t_{act}0.5$ are below the instrumental uncertainties for the system tested here. This is an important aspect for the application of the CSTR concept. An accurate determination of $P(t_{act})$, requires a sufficiently high time resolution throughout the whole experiment. This can be difficult to achieve depending on the type of instrument, e.g. scanning through different SS with the CCNC.

25   However, if a characterization of the aged aerosol during steady state is sufficiently precise, an accurate and therefore time intensive determination of the $P(t_{act})$ does not provide additional benefits.

Table 3 Comparison of t_{act} and $t_{act}0.5$ for both experiments.

	A: 1.0 % SS	B: 1.4 % SS
t_{act}	249.8 min	151.5 min
$t_{act}0.5 / \mu$	253.7 min	153.6 min
σ	35.5 min	24.6 min
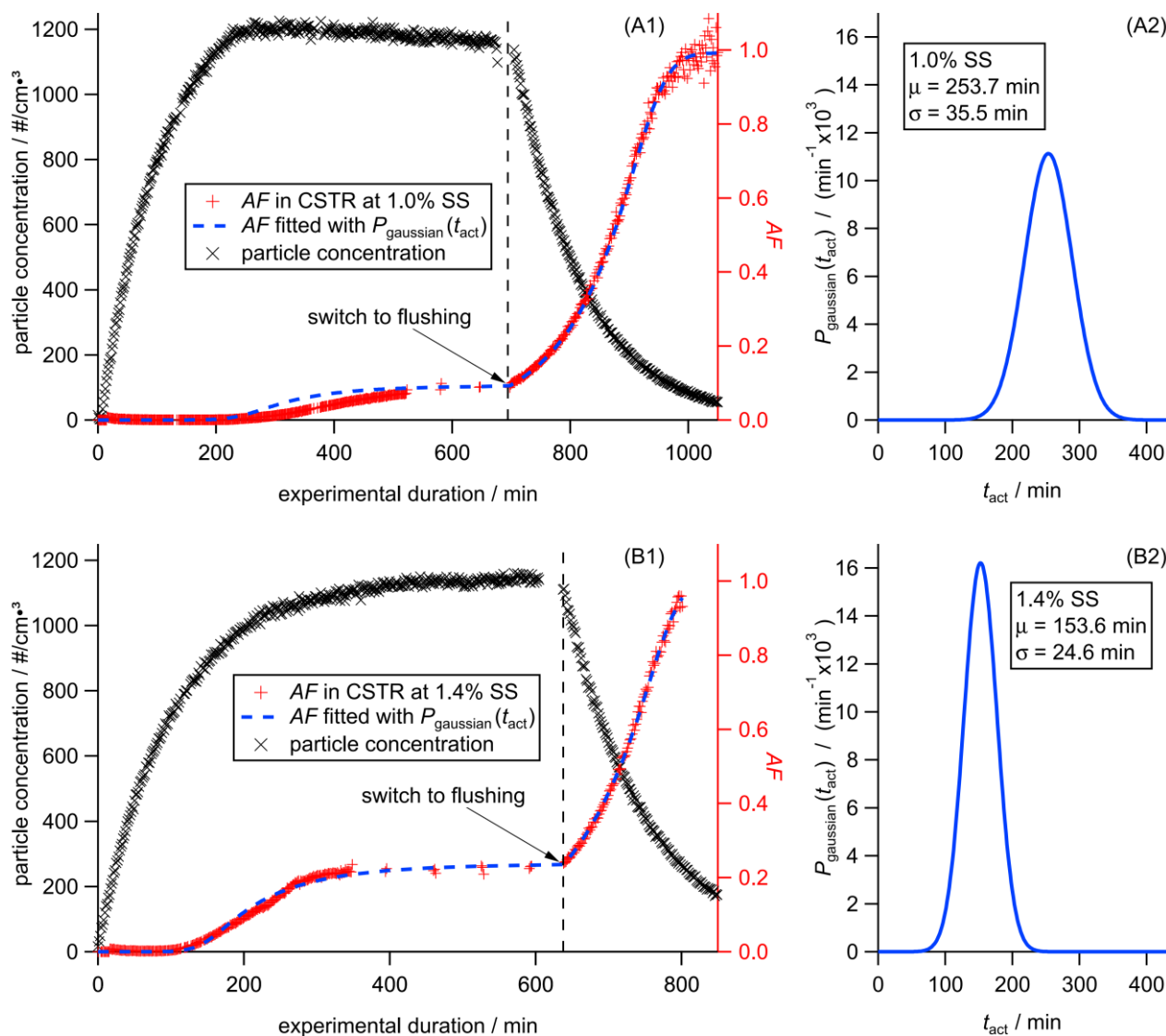
Figure 6: Particle concentration, measured *AF* (red crosses), fitted *AF* (blue dotted line; all A1/B1) and the corresponding activation time distributions $P(t_{act})$ (A2/B2) are shown.

6   Application of t_{act} to other continuous flow aerosol chambers

Besides various home-build OFRs (Keller and Burtscher, 2012; Ezell et al., 2010), the commercially available Potential Aerosol Mass Chamber (PAM, Aerodyne; Kang et al., 2007) has become an instrument widely used for the investigation of

aerosol aging in the recent years. Within these type of chambers an aerosol flow is exposed to OH-radicals. OH-radicals are typically produced by UV irradiation of ozone causing the production of excited oxygen atoms [$O(D^1)$] which react with water vapor. Within these type of chambers the OH-concentration tends to be significantly higher than the average atmospheric concentration in order to mimic several days of atmospheric aging in several minutes of experimental duration. For

5 intercomparison amongst chambers and for extrapolation to atmospheric conditions the total OH-exposure is used as a metric, which is often calculated by multiplying the OH-concentration with the exposure time. The exposure time is hereby equal to the residence time within the OFR which can be calculated the same way as in the CSTR-concept following eq. (1).

Lambe et al. (2011) performed an intercomparison of the Toronto Photo-Oxidation Tube (TPOT; George et al., 2007) and the PAM chamber. Here, the OH-exposure was determined from the SO_2-oxidation following eq. A1 in their paper. Amongst other

10 parameters, they investigated the secondary aerosol (SOA) formation from volatile organic compounds (VOCs) as well as the impact of heterogeneous oxidation on the CCN-activity of bis(2-ethylhexyl)sebacate (BES) particles. They found very good agreement concerning the average H/C and O/C ratios of the produced SOA particles and BES-particles. This indicates that the reaction with OH-radicals follows the same kinetic in both chambers. However, the CCN-activity of BES-particles aged in the PAM chamber is reported to be significantly higher than in the TPOT chamber at low OH-exposure levels and vice versa

15 at high OH-exposure levels as can be seen in Fig A2(a) in the respective publication. The authors identify differing residence time distributions between the two chambers and suggest a resulting difference in chemical composition that is not captured by the bulk H/C and O/C ratios to be the cause for the deviation in CCN-activity. In addition to major improvements in terms of operating the PAM chamber as well as in terms of analysis of PAM chamber data within the last couple of years, a range of modeling and experimental studies have been published investigating this specific aspect (e.g. Mitroo et al., 2018). In the

20 following we show that the application of t_{act} can contribute significantly to the explanation of the aforementioned discrepancies in terms of CCN-activity of the BES particles.

In Fig. 7 we show the RTDs for 145 nm BES particles using the parameters for the bimodal Taylor-dispersion model given by Lambe et al., (2011) in Appendix A4 (Fig A3). We normalize the area under the curve to be one causing the area under each curve to be directly proportional the AFs for a better visual comparison. Here, PAM chamber data is indicated by the dotted

25 line/green area and TPOT chamber data is indicated by the dashed line/blue area. As can be seen, the two curves are not perfectly superimposed with the peak of the PAM chamber RTD being earlier than in the TPOT chamber RTD followed by a steep decline causing the two curves to cross at approximately 40 s. Overall the PAM chamber RTD (dotted line) shows a stronger dispersion causing the two lines to cross again at approximately 180 s.
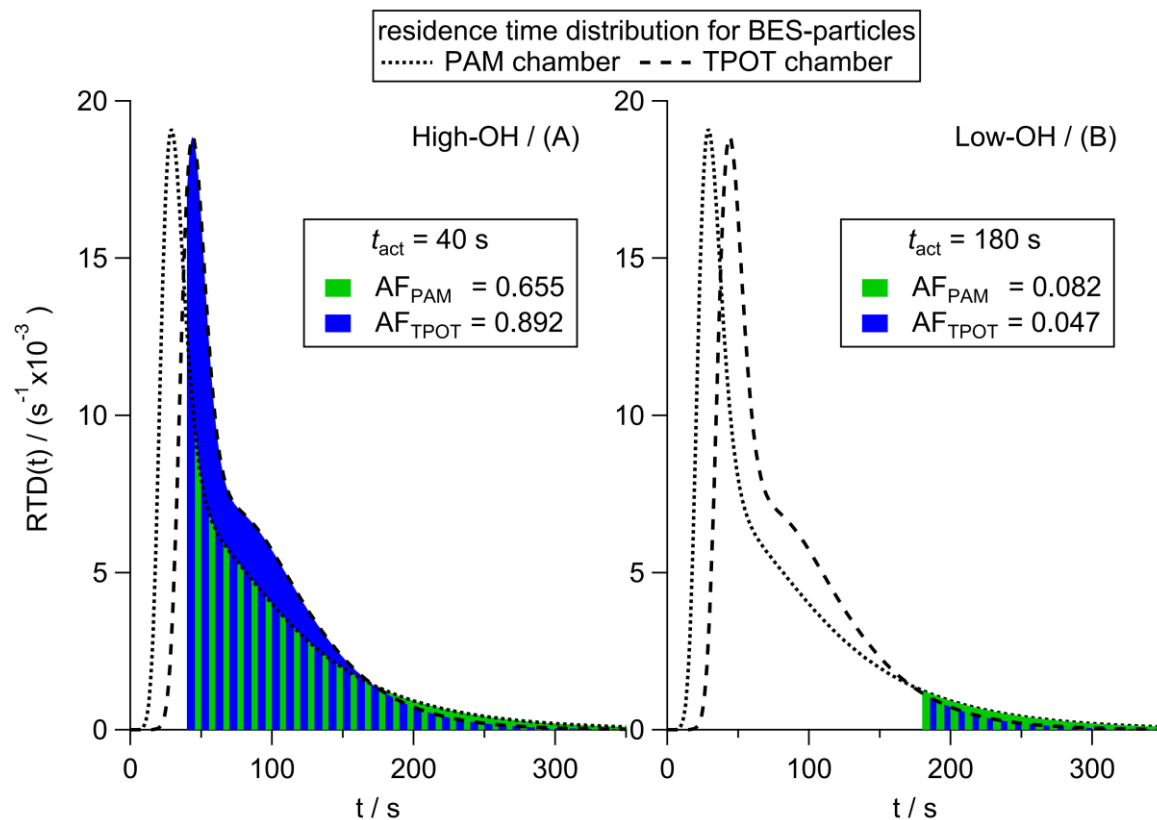
Figure 7: Global AF in the PAM and TPOT chamber for t_{act} of 40 and 180 s, respectively.

Assuming a high OH-concentration leads to a higher reaction speed and therefore shorter t_{act} we presente two scenarios. Scenario A is based on t_{act} of 40 s representing high OH-concentration (Fig. 7 A). The other scenario B is based on t_{act} of 180 s

5   representing low OH-concentration (Fig. 7 B). In both cases the BES-particles show CCN-activity, but the global AF differs significantly between both chamber types. While in the high-OH scenario A, the TPOT chamber is more efficient in producing CCN-active BES-particle ($AF_{TPOT} = 0.892$; blue area) than the PAM chamber ($AF_{PAM} = 0.655$; green area) as can be seen on the left, the PAM chamber is more efficient ($AF_{PAM} = 0.082$) than the TPOT chamber ($AF_{TPOT} = 0.047$) in case of the low-OH scenario B, as can be seen on the right. While the AF can differ between both chambers, other parameter can agree very well.

10   Such parameters could be the average H/C and O/C-ratios since the chemical modification of the aerosol is a continuous process. The CCN-activity is a function of this continuous chemical modification. However, once a certain modification threshold is reached no further increase in the CCN-activity of a single aerosol particle can be achieved at a constant SS. Therefore, AF does not linearly correlate with the average OH-exposure, but with the fraction of particles older than a certain t_{act}. At the same average OH-exposure, aging in different OFRs causes the same global AF only if the RTDs match. Three

15   examples of how t_{act} can deviate between the PAM and TPOT chamber at the same global AF are given in the supplement.

The discussion above ignores other processes in aging chambers such as particle wall-interaction and gas-phase-partitioning. Nevertheless, it explains why different OFR chamber measurements agree in some parameters dependent on the bulk properties of the aerosol particle population and at the same time disagree in other parameters, which are dependent on the condition/status of the individual particle (e.g. CCN-activity). This means, while the H/C and O/C-ratio determined by the AMS agree very well, measurements with a single particle instrument would result in a distribution of these ratios according to the RTD in the individual chamber. Depending on the parameter of interest we suggest using t_{act} or $P(t_{act})$ as metric.

7   Conclusion

This work investigated the potential of aerosol chambers operated in Continuous Flow Stirred Tank Reactor (CSTR) mode for simulating atmospheric aging processes of aerosol particles and retrieve data that is comparable to other methods. This approach was motivated by the possibility to achieve longer aging times in CSTR-mode than in batch-mode experiment in the same chamber at significantly lower aerosol concentration enabling the use of e.g. size selected aerosol particles. The main obstacle to implement this has hitherto been the residence time distribution inside the chamber, which results in a particle population consisting of particles at different aging stages. In order to address this, we introduced the activation time t_{act} as a new parameter to disentangle the non-uniform aerosol population and generate data that is comparable to other experimental setups. This concept was developed based on the assumption that continuous aging processes on the level of single particles can lead to a step-wise change in individual particle properties referred to as non-gradual transitions. The new parameter t_{act} describes the time needed to reach this transition. On a more fundamental level, t_{act} only requires a time-dependent change of a single particle property that can be used to distinguish between two states, below and above a defined threshold. Since particle properties are typically distributed around a mean value, we also introduced the activation time distribution $P(t_{act})$. The impact of t_{act} and $P(t_{act})$ on the measured parameters downstream an aerosol chamber was simulated with a newly developed mathematical framework and compared to experimental data. Data presented herein was acquired from experiments on soot particles transitioning form initial CCN-inactivity to CCN-activity over the course of several hours due to ozone exposure. We show that our theoretical concept describes the observed changes in the CCN-activity very well. Additionally, we show that the discrepancy between t_{act} and $t_{act}0.5$ is lower than the instrumental error in the model system in CSTR mode. Therefore, the data acquired during steady state is representative for the whole particle population. Finally, we generalize this concept and apply it to data of two other non-CSTR aging chambers published by Lambe et al. (2011). Through the application of our new concept we can explain qualitatively why the results from the PAM and TPOT chambers agree for some parameters (bulk O/C and H/C-ratio) but show significant differences for other parameters (CCN-activity; Lambe et al., 2011).

We recommend re-analysis of other ORF data to gain further insight to non-gradual transformation processes.

Author contribution.

FF and AAM wrote the manuscript and designed and carried out the experiments. FF developed the analysis concept and carried out the data analysis.

5 *Acknowledgements.*

This research was funded by the Swiss National Science Foundation; SNSF-grant #PZ00P2_161343. We thank Zamin A. Kanji, Oliver F. Bischof, Thomas Peter and Prem Lobo for their valuable discussions and the whole group of Ulrike Lohmann for their support.

10 *Data upload*

The data will be made available shortly.

Competing interests.

The authors declare that they have no conflict of interest.

15 **8   References**

Burkholder, J. B., Abbatt, J. P. D., Barnes, I., Roberts, J. M., Melamed, M. L., Ammann, M., Bertram, A. K., Cappa, C. D., Carlton, A. G., Carpenter, L. J., Crowley, J. N., Dubowski, Y., George, C., Heard, D. E., Herrmann, H., Keutsch, F. N., Kroll, J. H., McNeill, V. F., Ng, N. L., Nizkorodov, S. A., Orlando, J. J., Percival, C. J., Picquet-Varrault, B., Rudich, Y., Seakins, P. W., Surratt, J. D., Tanimoto, H., Thornton, J. A., Tong, Z., Tyndall, G. S., Wahner, A., Weschler, C. J., Wilson, K. R. and

20 Ziemann, P. J.: The Essential Role for Laboratory Studies in Atmospheric Chemistry, Environ. Sci. Technol., 51(5), 2519–2528, doi:10.1021/acs.est.6b04947, 2017.

Cholette, A. and Cloutier, L.: Mixing efficiency determinations for continuous flow systems, Can. J. Chem. Eng., 37(3), 105–112, doi:10.1002/cjce.5450370305, 1959.

Crump, J. G. and Seinfeld, J. H.: Aerosol Behaviour in The Continous Stirred Tank Reactor, Am. Inst. Chem. Eng., 26(4),

25 1980.

Donahue, N. M., Robinson, A. L., Stanier, C. O. and Pandis, S. N.: Coupled partitioning, dilution, and chemical aging of semivolatile organics, Environ. Sci. Technol., 40(8), 2635–2643, doi:10.1021/es052297c, 2006.

Ezell, M. J., Johnson, S. N., Yu, Y., Perraud, V., Bruns, E. A., Alexander, M. L., Zelenyuk, A., Dabdub, D. and Finlayson-Pitts, B. J.: A new aerosol flow system for photochemical and thermal studies of tropospheric aerosols, Aerosol Sci. Technol.,

30 44(5), 329–338, doi:10.1080/02786821003639700, 2010.

George, I. J., Vlasenko, A., Slowik, J. G., Broekhuizen, K. and Abbatt, J. P. D.: Heterogeneous oxidation of saturated organic aerosols by hydroxyl radicals: Uptake kinetics, condensed-phase products, and particle size change, Atmos. Chem. Phys.,

7(16), 4187–4201, doi:10.5194/acp-7-4187-2007, 2007.

Kang, E., Root, M. J., Toohey, D. W. and Brune, W. H.: Introducing the concept of Potential Aerosol Mass (PAM), Atmos. Chem. Phys., 7(22), 5727–5744, doi:10.5194/acp-7-5727-2007, 2007.

Keller, A. and Burtscher, H.: A continuous photo-oxidation flow reactor for a defined measurement of the SOA formation potential of wood burning emissions, J. Aerosol Sci., 49(November 2016), 9–20, doi:10.1016/j.jaerosci.2012.02.007, 2012.

Kuwata, M. and Martin, S. T.: Particle Size Distributions following Condensational Growth in Continuous Flow Aerosol Reactors as Derived from Residence Time Distributions: Theoretical Development and Application to Secondary Organic Aerosol, Aerosol Sci. Technol., 46(8), 937–949, doi:10.1080/02786826.2012.683204, 2012.

Lambe, A. T., Ahern, A. T., Williams, L. R., Slowik, J. G., Wong, J. P. S., Abbatt, J. P. D., Brune, W. H., Ng, N. L., Wright, J. P., Croasdale, D. R., Worsnop, D. R., Davidovits, P. and Onasch, T. B. B.: Characterization of aerosol photooxidation flow reactors: Heterogeneous oxidation, secondary organic aerosol formation and cloud condensation nuclei activity measurements, Atmos. Meas. Tech., 4(3), 445–461, doi:10.5194/amt-4-445-2011, 2011.

McNeill, V. F., Wolfe, G. M. and Thornton, J. A.: The oxidation of oleate in submicron aqueous salt aerosols: Evidence of a surface process, J. Phys. Chem. A, 111(6), 1073–1083, doi:10.1021/jp066233f, 2007.

Mitroo, D., Sun, Y., Combest, D. P., Kumar, P. and Williams, B. J.: Assessing the degree of plug flow in oxidation flow reactors (OFRs): A study on a potential aerosol mass (PAM) reactor, Atmos. Meas. Tech., 11(3), 1741–1756, doi:10.5194/amt-11-1741-2018, 2018.

Roberts, G. C. and Nenes, a.: A Continuous-Flow Streamwise Thermal-Gradient CCN Chamber for Atmospheric Measurements, Aerosol Sci. Technol., 39(3), 206–221, doi:10.1080/027868290913988, 2005.

Rohrer, F., Bohn, B., Brauers, T., Brüning, D., Johnen, F.-J., Wahner, A. and Kleffmann, J.: Characterisation of the photolytic HONO-source in the atmosphere simulation chamber SAPHIR, Atmos. Chem. Phys., 5(8), 2189–2201, doi:10.5194/acp-5-2189-2005, 2005.

Rollins, A. W., Kiendler-Scharr, A., Fry, J. L., Brauers, T., Brown, S. S., Dorn, H. P., Dubé, W. P., Fuchs, H., Mensah, A., Mentel, T. F., Rohrer, F., Tillmann, R., Wegener, R., Wooldridge, P. J. and Cohen, R. C.: Isoprene oxidation by nitrate radical: Alkyl nitrate and secondary organic aerosol yields, Atmos. Chem. Phys., 9(18), 6685–6703, doi:10.5194/acp-9-6685-2009, 2009.

Textor, C., Schulz, M., Guibert, S., Kinne, S., Balkanski, Y., Bauer, S., Berntsen, T., Berglen, T., Boucher, O., Chin, M., Dentener, F., Diehl, T., Easter, R., Feichter, H., Fillmore, D., Ghan, S., Ginoux, P., Gong, S., Grini, A., Hendricks, J., Horowitz, L., Huang, P., Isaksen, I., Iversen, T., Kloster, S., Koch, D., Kirkevåg, A., Kristjansson, J. E., Krol, M., Lauer, A., Lamarque, J. F., Liu, X., Montanaro, V., Myhre, G., Penner, J., Pitari, G., Reddy, S., Seland, Stier, P., Takemura, T. and Tie, X.: Analysis and quantification of the diversities of aerosol life cycles within AeroCom, Atmos. Chem. Phys., 6(7), 1777–1813, doi:10.5194/acp-6-1777-2006, 2006.